

Triplon-mediated pairing and the superconducting gap structure in bilayer nickelates

Huimei Liu^{1,2} and Giniyat Khaliullin³

¹*National Laboratory of Solid State Microstructures and School of Physics, Nanjing University, Nanjing 210093, China*

²*Collaborative Innovation Center of Advanced Microstructures, Nanjing University, Nanjing 210093, China*

³*Max Planck Institute for Solid State Research, Heisenbergstrasse 1, D-70569 Stuttgart, Germany*

(Dated: March 2, 2026)

We investigate the superconducting gap structure in bilayer nickelates within a model where conduction bands of $d_{x^2-y^2}$ symmetry coexist with localized $d_{3z^2-r^2}$ spins. Strong interlayer coupling drives the local moments into a singlet ground state, whose virtual singlet–triplet excitations (“triplons”) mediate the pairing interaction between conduction electrons. This yields interband s_{\pm} pairing, with opposite signs of the order parameter on the bonding β and antibonding α bands. Our theory naturally explains two key experimental features: a larger gap on the α band despite its smaller density of states, and pronounced gap anisotropy arising from momentum-dependent nonlocal Kondo coupling. These results support triplon-mediated pairing as the microscopic origin of superconductivity in bilayer nickelates.

The recent discovery of superconductivity in bilayer nickelates under high pressure and epitaxial strain has opened a new frontier in the study of unconventional high- T_c superconductors [1–6]. Different from cuprates, where superconductivity emerges from a single half-filled $d_{x^2-y^2}$ orbital, bilayer nickelates involve a mixed-valence $\text{Ni}^{2.5+}$ state with active $d_{x^2-y^2}$ and $d_{3z^2-r^2}$ orbitals, fundamentally altering the nature of low-energy correlations and pairing. The interplay of orbital physics, strong interlayer coupling, electron correlations, and lattice effects creates a complex theoretical landscape, and the nature of pairing mechanisms in nickelates remains under active debate (see, e.g., [7–21] and references therein).

Recent experiments have reported the superconducting gaps in bilayer nickelate thin films [22–24] and bulk $\text{La}_3\text{Ni}_2\text{O}_{7-\delta}$ under pressure [25, 26]. The two distinct superconducting gaps have been resolved [22, 25]. These gaps can be associated with the bonding and antibonding bands intrinsic to a bilayer structure. It is particularly striking that the band with the smaller density of states at the Fermi level hosts the larger superconducting gap, and both gaps display a pronounced angular anisotropy [22]. These observations impose strong constraints on the theoretical models and pairing mechanisms.

In this Letter, we present a theory that accounts for these experimental observations. Building on the earlier proposal that interlayer singlet–triplet excitations (“triplons”) of the localized $d_{3z^2-r^2}$ electrons can mediate the pairing interaction [20], we develop a microscopic model which quantifies the superconducting gap structure in bilayer nickelates. We formulate a tight-binding description of the bilayer-split bands and derive the effective interactions between localized spins and itinerant electrons arising from intraionic Hund’s coupling and intersite Kondo exchange. The resulting BCS Hamiltonian exhibits a distinctive spin and band-flavor structure, leading naturally to interband s_{\pm} pairing with opposite signs and different amplitudes of the order parameter on

the bonding and antibonding bands. The calculated gap values are anisotropic in momentum space, due to the Kondo exchange contribution to the pairing interaction. Our results are fully consistent with the observed gap hierarchy and angular dependence, providing strong support for triplon-mediated pairing in this new family of unconventional superconductors.

The model: spin-dimers, triplons, and conduction bands.—In bilayer nickelates, the nominal valence of Ni is close to $\text{Ni}^{2.5+}$, corresponding to an average $d^{7.5}$ configuration. Consequently, the e_g manifold contains about 1.5 electrons per Ni. The tetragonal crystal field lifts the e_g degeneracy, splitting the levels into a lower $d_{3z^2-r^2}$ orbital and a higher $d_{x^2-y^2}$ orbital. With sufficiently large orbital splitting of the order of 1 eV, as realized, e.g., in the ab -plane compressed superconducting thin films [19, 27], one electron per Ni predominantly occupies the $d_{3z^2-r^2}$ orbital, giving rise to a localized spin- $\frac{1}{2}$ moment. The remaining ~ 0.5 electron contributes to itinerant carriers forming wide conduction bands of $d_{x^2-y^2}$ symmetry.

Large overlap of the $d_{3z^2-r^2}$ orbitals on the c axis bonds results in a strong interlayer spin interaction $\mathcal{H}_c = J_c(\mathbf{S}_1 \cdot \mathbf{S}_2)$ with $J_c = 4t_c^2/U$, where $t_c \sim 0.6$ eV and $U \sim 5$ eV are the hopping integral and intraionic Coulomb repulsion, respectively. This stabilizes an interlayer singlet ground state separated by a finite gap of $J_c \sim 0.3$ eV from the triplet level, as shown in Fig. 1 (a). Singlet-to-triplet spin excitations—dubbed “triplons”—are nearly local objects because the ab -plane hopping of $d_{3z^2-r^2}$ orbitals $t_{ab} \sim t_c/4$ and the corresponding exchange coupling $J_{ab} \sim (t_{ab}/t_c)^2 J_c$ are very small. In essence, the local spins $S = 1/2$ hosted by $d_{3z^2-r^2}$ orbitals form a bilayer antiferromagnet in its singlet phase, and the spin excitations are described by hard-core vector bosons \mathbf{T} with weakly dispersive energy relation $\omega_{\mathbf{q}} \simeq J_c + J_{ab}(\cos q_x + \cos q_y) \sim J_c$ [20].

Next we address the conduction bands in a bilayer structure. While direct overlap of the planar $d_{x^2-y^2}$ orbitals on the c axis bonds is negligible, there are a num-

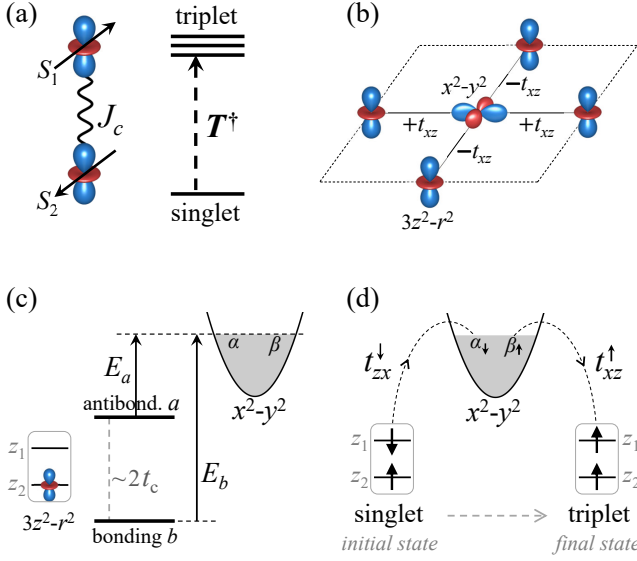


FIG. 1. (a) On the c axis bond connecting two layers 1 and 2, the localized $d_{3z^2-r^2}$ spins S_1 and S_2 interact via antiferromagnetic coupling $J_c = 4t_c^2/U$ and form a spin-dimer with singlet ground state. Singlet-to-triplet excitation (dashed arrow) with energy J_c is described by a boson creation operator T^\dagger . (b) In-plane hopping geometry between itinerant $d_{x^2-y^2}$ and local $d_{3z^2-r^2}$ orbitals. The opposite signs of $\pm t_{xz}$ along the x and y bonds generates $\eta_{\mathbf{k}} = \cos k_x - \cos k_y$ structure in momentum space. (c) In the virtual hopping process $d_{3z^2-r^2} \rightarrow d_{x^2-y^2}$, the $\langle z_1; z_2 \rangle$ dimer is left with a single $d_{3z^2-r^2}$ electron in the intermediate state, forming bonding b and antibonding a molecular orbitals with energies E_b and E_a below the Fermi level. Owing to the different excitation energies in the bonding $b \rightarrow \beta$ and antibonding $a \rightarrow \alpha$ hopping channels, the initially degenerate β and α bands obtain different self-energy corrections and will thus split. (d) Illustration of the Kondo exchange process where virtual t_{zx} hoppings generate on-site singlet-to-triplet transition (triplon T_1^\dagger with $S_z = 1$ is created in the case shown).

ber of indirect interlayer hopping paths via other orbital states. A natural channel in the present case is the indirect hopping t_{xz} via $d_{3z^2-r^2}$ states as we consider now.

Using shorthand notations z and x for the localized $d_{3z^2-r^2}$ and itinerant $d_{x^2-y^2}$ orbitals, respectively, the interorbital t_{xz} hopping Hamiltonian is written as

$$\mathcal{H}_{xz} = \sum_{i,\delta} (\pm) t_{xz} (x_{1,i}^\dagger z_{1,i+\delta} + x_{2,i}^\dagger z_{2,i+\delta} + H.c.), \quad (1)$$

where the \pm sign reflects the opposite phases of the $d_{x^2-y^2}$ orbital along the $\delta = x$ and $\delta = y$ bond directions as shown in Fig. 1 (b), and the index 1, 2 labels two layers.

We introduce bonding β and antibonding α conduction bands $\beta/\alpha = \frac{1}{\sqrt{2}}(x_1 \pm x_2)$, and similarly, the interlayer $d_{3z^2-r^2}$ molecular orbitals $b/a = \frac{1}{\sqrt{2}}(z_1 \pm z_2)$. In this

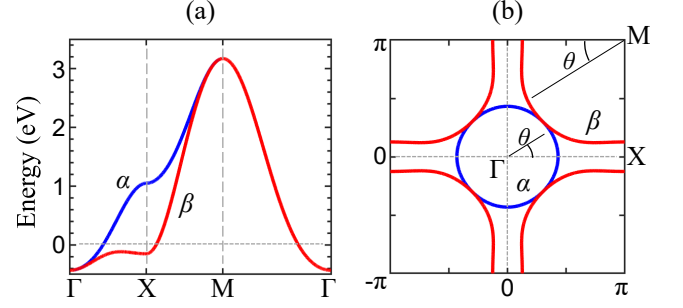


FIG. 2. (a) Antibonding α (blue) and bonding β (red) band dispersions along $\Gamma(0,0)$ — $X(\pi,0)$ — $M(\pi,\pi)$ path, and (b) the corresponding Fermi surfaces in the Brillouin zone. The model parameters are $t_1 = 0.45$, $t_2 = -0.24$, $t_3 = 0.06$, $\epsilon_\alpha = 0.4$, and $\epsilon_\beta = 0.1$ (in units of eV). The chemical potential $\mu = -0.65$ eV is chosen to obtain the band fillings (per Ni ion) $n_\alpha = 0.14$ and $n_\beta = 0.31$ (as reported in ARPES study [24]).

basis, Eq. (1) reads in momentum space as

$$\mathcal{H}_{xz} = 2t_{xz} \sum_{\mathbf{k}} \eta_{\mathbf{k}} (\beta_{\mathbf{k}}^\dagger b_{\mathbf{k}} + \alpha_{\mathbf{k}}^\dagger a_{\mathbf{k}} + H.c.), \quad (2)$$

where $\eta_{\mathbf{k}} = \cos k_x - \cos k_y$. This Hamiltonian describes hybridization between localized z and band x states in the even and odd parity channels (with respect to the bilayer mirror symmetry). The key point is that the excitation energies in these two channels greatly differ, due to large interlayer splitting between bonding b and antibonding a molecular orbitals of the order of $2t_c \sim 1.2$ eV, as illustrated in Fig. 1 (c). While removing an electron from a singly-occupied a orbital costs energy E_a , the excitation energy in the bonding channel $b \rightarrow \beta$ is much larger, $E_b \sim E_a + 2t_c$. This results in different self-energy corrections $\delta\xi_{\mathbf{k}}$ to the α and β band dispersions:

$$\begin{aligned} \delta\xi_{\alpha\mathbf{k}} &= \epsilon_\alpha \eta_{\mathbf{k}}^2 & \text{with} & \quad \epsilon_\alpha = 4t_{xz}^2 \left(\frac{1}{E_a} - \frac{1}{E_a + U} \right), \\ \delta\xi_{\beta\mathbf{k}} &= \epsilon_\beta \eta_{\mathbf{k}}^2 & \text{with} & \quad \epsilon_\beta = 4t_{xz}^2 \left(\frac{1}{E_b} - \frac{1}{E_b + U} \right). \end{aligned} \quad (3)$$

Here, $E_{a/b} + U$ is the energy required to add an electron to a singly-occupied $d_{3z^2-r^2}$ level; as $U \sim 5$ eV is large, this process is less important and not shown in Fig. 1.

The Hamiltonian for conduction bands becomes

$$\mathcal{H}_c = \sum_{\mathbf{k}} (\xi_{\alpha\mathbf{k}} \alpha_{\mathbf{k}}^\dagger \alpha_{\mathbf{k}} + \xi_{\beta\mathbf{k}} \beta_{\mathbf{k}}^\dagger \beta_{\mathbf{k}}), \quad (4)$$

with the dispersion relations

$$\xi_{\alpha/\beta,\mathbf{k}} = -4(t_1\gamma_{1\mathbf{k}} + t_2\gamma_{2\mathbf{k}} + t_3\gamma_{3\mathbf{k}}) + \epsilon_{\alpha/\beta}\eta_{\mathbf{k}}^2 - \mu. \quad (5)$$

Here $t_{1,2,3}$ are the in-plane tight-binding hopping parameters up to the third neighbors, $\gamma_{1\mathbf{k}} = \frac{1}{2}(\cos k_x + \cos k_y)$, $\gamma_{2\mathbf{k}} = \cos k_x \cos k_y$, $\gamma_{3\mathbf{k}} = \frac{1}{2}(\cos 2k_x + \cos 2k_y)$, and μ is

the chemical potential. As argued above, $\epsilon_\alpha > \epsilon_\beta$, thus the initial degeneracy of two bands is lifted.

In principle, one may also consider the other virtual processes, such as the $4s$ -orbital admixtures that would contribute to $\xi_{\mathbf{k}}$ with the same $\eta_{\mathbf{k}}^2$ factor, longer-range interlayer hoppings, etc. Here we use Eq. (5) considering $\epsilon_{\alpha/\beta}$ as free parameters. The representative α and β band dispersions and corresponding Fermi surfaces are shown in Fig. 2, which are consistent with the density functional theory calculations [7] and ARPES data in bilayer nickelate thin films [24, 28].

Up to now, we described the basic ingredients of the model: triplons \mathbf{T} with energy $\omega_{\mathbf{q}} \sim J_c$, and conduction bands $\alpha_{\mathbf{k}}$ and $\beta_{\mathbf{k}}$ with dispersions (5). Next, we discuss interactions between these degrees of freedom.

Interactions between the local and itinerant electron spins.—We consider the following spin exchange mechanisms.

(i) The intraionic Hund's coupling between local \mathbf{S} and itinerant \mathbf{s} spins. In a bilayer system, it reads as:

$$\mathcal{H}_H = -2J_H \sum_i [(\mathbf{S} \cdot \mathbf{s})_1 + (\mathbf{S} \cdot \mathbf{s})_2]_i. \quad (6)$$

We express local spins via triplon \mathbf{T} operators [29, 30]:

$$\mathbf{S}_{1,2} = \pm \frac{1}{2}(\mathbf{T} + \mathbf{T}^\dagger) - \frac{i}{2}(\mathbf{T}^\dagger \times \mathbf{T}), \quad (7)$$

where upper/lower sign refers to the first/second layer. In singlet phase where the triplons are gapped and hence their density is small, we may keep only \mathbf{T} -linear terms in Eq. (6). It follows that triplons couple to the odd-parity combination of band spins $(\mathbf{s}_1 - \mathbf{s}_2) = (\mathbf{s}_{\alpha\beta} + \mathbf{s}_{\beta\alpha})$:

$$\mathcal{H}_H = -J_H \sum_{\mathbf{k}\mathbf{k}'} (\mathbf{T}_{\mathbf{q}} + \mathbf{T}_{-\mathbf{q}}^\dagger) \cdot (\mathbf{s}_{\alpha\beta}^{\mathbf{k}'\mathbf{k}} + \mathbf{s}_{\beta\alpha}^{\mathbf{k}'\mathbf{k}}). \quad (8)$$

The interband spin density $\mathbf{s}_{\alpha\beta}^{\mathbf{k}'\mathbf{k}} = \frac{1}{2}\alpha_{\mathbf{k}'s'}^\dagger \boldsymbol{\sigma}_{s's} \beta_{\mathbf{k}s}$, where $\boldsymbol{\sigma}$ are the Pauli matrices and $\mathbf{q} = \mathbf{k}' - \mathbf{k}$.

(ii) The antiferromagnetic Kondo coupling generated by virtual hoppings between local and conduction electrons [31]. As illustrated in Fig. 1(d), a triplon is created by the t_{zx} hopping processes; this is accompanied by spin-orbital flip $\alpha_{\downarrow}^\dagger \beta_{\uparrow}$ in the band sector, as required by spin-and-parity symmetry. We obtain

$$\mathcal{H}_K = \sum_{\mathbf{k}\mathbf{k}'} [\eta_{\mathbf{k}} \eta_{\mathbf{k}'} (J_K^a \mathbf{T}_{\mathbf{q}} + J_K^b \mathbf{T}_{-\mathbf{q}}^\dagger) \mathbf{s}_{\alpha\beta}^{\mathbf{k}'\mathbf{k}} + H.c.], \quad (9)$$

where

$$\begin{aligned} J_K^a &= 4t_{xz}^2 \left(\frac{1}{E_a} + \frac{1}{E_a + U} \right), \\ J_K^b &= 4t_{xz}^2 \left(\frac{1}{E_b} + \frac{1}{E_b + U} \right). \end{aligned} \quad (10)$$

Two different exchange constants with $J_K^a > J_K^b$ appear due to bonding-antibonding splitting of the $d_{3z^2-r^2}$ levels

in the intermediate state, i.e., for the same reason as in the density channel above, cf. Eq. (3).

The total interaction $\mathcal{H}_K + \mathcal{H}_H$ between singlet-triplet excitations \mathbf{T} and itinerant spins reads then as follows:

$$\mathcal{H}_{\text{int}} = -J_H \sum_{\mathbf{k}\mathbf{k}'} [(f_{\mathbf{k}\mathbf{k}'}^a \mathbf{T}_{\mathbf{q}} + f_{\mathbf{k}\mathbf{k}'}^b \mathbf{T}_{-\mathbf{q}}^\dagger) \mathbf{s}_{\alpha\beta}^{\mathbf{k}'\mathbf{k}} + H.c.], \quad (11)$$

where $f_{\mathbf{k}\mathbf{k}'}^a = (1 - \kappa_a \eta_{\mathbf{k}} \eta_{\mathbf{k}'})$ and $f_{\mathbf{k}\mathbf{k}'}^b = (1 - \kappa_b \eta_{\mathbf{k}} \eta_{\mathbf{k}'})$. The parameters $\kappa_a = J_K^a/J_H$ and $\kappa_b = J_K^b/J_H$ quantify strength of the intersite Kondo exchange relative to intraionic Hund's coupling. The κ -terms bring about non-local character of the interactions; as shown below, they are instrumental in explanation of the superconducting gap structure observed in bilayer nickelates.

Few comments are in order here. We assume that the ferromagnetic Hund's coupling is strong enough to prevent Kondo instability and related heavy fermion physics. On the other hand, we assume that Hund's splitting $2J_H$ in nickelates is well below the e_g electron bandwidth of $W \sim 3 - 4$ eV, i.e., it is not strong enough to form $S = 1$ local spins and stabilize their magnetic ordering by virtue of double exchange mechanism. Under these assumptions, we will treat \mathcal{H}_{int} of Eq. (11) perturbatively.

Finally, different from the spin-fermion models widely used in the context of superconductivity in correlated electron systems, spin fluctuations in Hamiltonian (11) are represented by weakly dispersive singlet-triplet excitations \mathbf{T} . Unlike (over)damped paramagnons in standard spin-fluctuation theories, triplons are quasi-local modes with high energies $J_c \sim 0.3$ eV, thanks to strong interlayer overlap of the $d_{3z^2-r^2}$ orbitals. Experimentally, triplons are detectable by inelastic neutron and resonant x-ray scattering, with the largest intensity at $q_z = \pi$.

Cooper pairing and the gap structure.—The exchange of triplet excitations with energy $\sim J_c$ generates an effective interaction between itinerant electrons [20]. Treating Eq. (11) in a second-order perturbation theory, we obtain the interband pairing interaction:

$$\mathcal{H}_{\text{BCS}} = \sum_{\mathbf{k}\mathbf{k}'} V_{\mathbf{k}\mathbf{k}'} (\alpha_{\mathbf{k}\uparrow}^\dagger \alpha_{-\mathbf{k}\downarrow}^\dagger \beta_{-\mathbf{k}'\downarrow} \beta_{\mathbf{k}'\uparrow} + H.c.), \quad (12)$$

with the momentum dependent matrix element

$$V_{\mathbf{k}\mathbf{k}'} = V f_{\mathbf{k}\mathbf{k}'}^a f_{\mathbf{k}\mathbf{k}'}^b = V (1 - \kappa_a \eta_{\mathbf{k}} \eta_{\mathbf{k}'}) (1 - \kappa_b \eta_{\mathbf{k}} \eta_{\mathbf{k}'}). \quad (13)$$

The coupling constant $V = 3J_H^2/2J_c$. One may notice here that J_H and J_c formally correspond to the electron-phonon coupling strength and phonon energy, respectively, in the phonon-mediated pairing theory.

BCS mean-field treatment of the interaction (12) leads to the following equations for the pairing gaps $\Delta_{\alpha\mathbf{k}}$ and $\Delta_{\beta\mathbf{k}}$ on the α and β Fermi-surfaces:

$$\begin{aligned} \Delta_{\alpha\mathbf{k}} &= - \sum_{\mathbf{k}'} V_{\mathbf{k}\mathbf{k}'} \frac{\Delta_{\beta\mathbf{k}'}}{2\varepsilon_{\beta\mathbf{k}'}} \tanh \frac{\varepsilon_{\beta\mathbf{k}'}}{2T}, \\ \Delta_{\beta\mathbf{k}} &= - \sum_{\mathbf{k}'} V_{\mathbf{k}\mathbf{k}'} \frac{\Delta_{\alpha\mathbf{k}'}}{2\varepsilon_{\alpha\mathbf{k}'}} \tanh \frac{\varepsilon_{\alpha\mathbf{k}'}}{2T}. \end{aligned} \quad (14)$$

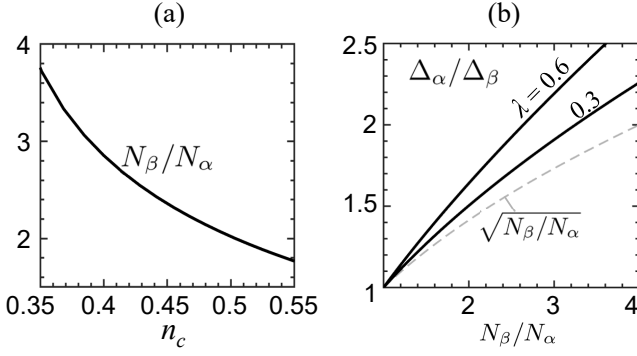


FIG. 3. (a) Ratio N_β/N_α of the DOS at the Fermi level for α and β bands of Fig. 2 as a function of electron density (per Ni) $n_c = n_\alpha + n_\beta$. (b) Ratio of superconducting gap amplitudes $\Delta_\alpha/\Delta_\beta$ as a function of N_β/N_α , following from Eq. (18) at $\lambda = 0.6$ and 0.3 . Dashed line $\sqrt{N_\beta/N_\alpha}$ shows $\lambda \rightarrow 0$ limit.

The quasiparticle energies $\varepsilon_{\alpha\mathbf{k}} = \sqrt{\xi_{\alpha\mathbf{k}}^2 + \Delta_{\alpha\mathbf{k}}^2}$ and $\varepsilon_{\beta\mathbf{k}} = \sqrt{\xi_{\beta\mathbf{k}}^2 + \Delta_{\beta\mathbf{k}}^2}$ with $\xi_{\alpha/\beta}$ from Eq. (5). The two gap equations are coupled, reflecting the interband pairing nature of the interactions in Eq. (12).

The leading solution of Eq. (14) corresponds to a so-called interband s_\pm -wave state, in which the gaps on the α and β Fermi surfaces have opposite signs, e.g., $\text{sgn}(\Delta_\alpha) = -\text{sgn}(\Delta_\beta)$. In the following, we omit the signs of the gaps and focus on only their magnitudes: $\Delta_{\alpha/\beta} = |\Delta_{\alpha/\beta}|$. By s -wave symmetry, the κ -linear terms in $V_{\mathbf{k}\mathbf{k}'}$ drop out under momentum summation in Eq. (14), and the gap equations at $T = 0$ read as

$$\begin{aligned}\Delta_{\alpha\mathbf{k}} &= V \sum_{\mathbf{p}} (1 + \kappa^2 \eta_{\mathbf{k}}^2 \eta_{\mathbf{p}}^2) \frac{\Delta_{\beta\mathbf{p}}}{2\varepsilon_{\beta\mathbf{p}}}, \\ \Delta_{\beta\mathbf{k}} &= V \sum_{\mathbf{p}} (1 + \kappa^2 \eta_{\mathbf{k}}^2 \eta_{\mathbf{p}}^2) \frac{\Delta_{\alpha\mathbf{p}}}{2\varepsilon_{\alpha\mathbf{p}}},\end{aligned}\quad (15)$$

where $\kappa^2 = \kappa_a \kappa_b = J_K^a J_K^b / J_H^2$.

Approximating the momentum summations in Eq. (15) by integrals around the Fermi level (with upper energy cutoff $\Omega \sim J_c$), we find $\sum_{\mathbf{p}} (\Delta_{\mathbf{p}}/2\varepsilon_{\mathbf{p}}) \approx N \Delta \ln \frac{2\Omega}{\Delta}$ and $\sum_{\mathbf{p}} \eta_{\mathbf{p}}^2 (\Delta_{\mathbf{p}}/2\varepsilon_{\mathbf{p}}) \approx \tilde{N} \Delta \ln \frac{2\Omega}{\Delta}$, where N is the density of states (DOS) at the Fermi level, while \tilde{N} denotes the DOS weighted by $\eta_{\mathbf{k}}^2$. This results in the following momentum dependence of the pairing gaps:

$$\begin{aligned}\Delta_{\alpha\mathbf{k}} &= \Delta_\alpha \left[1 + \frac{\tilde{N}_\beta}{N_\beta} \kappa^2 \eta_{\mathbf{k}}^2 \right], \\ \Delta_{\beta\mathbf{k}} &= \Delta_\beta \left[1 + \frac{\tilde{N}_\alpha}{N_\alpha} \kappa^2 \eta_{\mathbf{k}}^2 \right],\end{aligned}\quad (16)$$

where

$$\Delta_\alpha = V N_\beta \Delta_\beta \ln \frac{2\Omega}{\Delta_\beta} \quad \text{and} \quad \Delta_\beta = V N_\alpha \Delta_\alpha \ln \frac{2\Omega}{\Delta_\alpha} \quad (17)$$

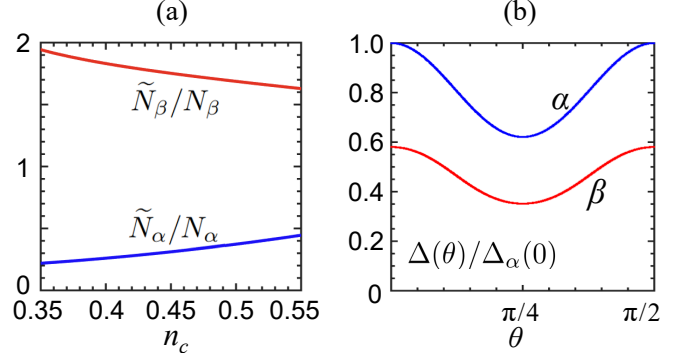


FIG. 4. (a) \tilde{N}/N ratio (i.e. density of states \tilde{N} weighted by $\eta_{\mathbf{k}}^2$ factor relative to N) as a function of electron density n_c per Ni ion. (b) Superconducting gap values (relative to Δ_α at $\theta = 0$) at the α and β Fermi surfaces as a function of angle θ [which is defined in Fig. 2(b)], calculated from Eqs. (16) and (18) with $n_c = 0.45$, $\kappa = 0.75$, and $\lambda = 0.5$.

are the coupled equations for Δ_α and Δ_β along the diagonal $\theta = \pi/4$ direction, where $\eta_{\mathbf{k}} = \cos k_x - \cos k_y = 0$.

The ratio of gap magnitudes between the two Fermi surface sheets is estimated from Eq. (17) as

$$\frac{\Delta_\alpha}{\Delta_\beta} = \left(\frac{N_\beta}{N_\alpha} \right)^{\frac{1}{2}} \left[\frac{\ln(2\Omega/\Delta_\beta)}{\ln(2\Omega/\Delta_\alpha)} \right]^{\frac{1}{2}} \simeq \left(\frac{N_\beta}{N_\alpha} \right)^{\frac{1}{2-\lambda}}, \quad (18)$$

where $\lambda = V \sqrt{N_\alpha N_\beta} = \sqrt{\lambda_\alpha \lambda_\beta}$. This approximation is valid if $\lambda \ln \frac{\Delta_\alpha}{\Delta_\beta} < 2$, which is well satisfied for small λ values assumed in this study. From Eq. (17), it also follows that $\Delta \approx 2\Omega \exp(-1/\lambda)$, where $\Delta = \sqrt{\Delta_\alpha \Delta_\beta}$.

The ratio N_β/N_α depends on the band structure parameters, and also on the electron density n_c as shown in Fig. 3 (a). The evolution of N_β/N_α strongly impacts the gap hierarchy, leading to large changes in $\Delta_\alpha/\Delta_\beta$ ratio, see Fig. 3(b). Interestingly, the larger gap emerges on the α -sheet despite its smaller DOS at the Fermi level. This counterintuitive observation originates from the interband nature of the triplon-mediated pairing.

According to Eq. (16), anisotropy of the superconducting gap $\Delta_{\alpha\mathbf{k}}$ on the α band depends on the ratio \tilde{N}_β/N_β of the “weighted” to “bare” density of states on the β -sheet, and vice versa. The \tilde{N}/N values depend on the band filling, see Fig. 4(a). We recall that the gap anisotropy is due to nonlocal Kondo coupling, represented by the κ terms in the pairing potential $V_{\mathbf{k}\mathbf{k}'}$ (13).

Figure 4(b) represents the superconducting gap structure, calculated using the bands and Fermi surfaces of Fig. 2. While quantitative details depend on the parameters used, its basic features such as the gap hierarchy of $\Delta_\alpha > \Delta_\beta$ and large angular anisotropy are the robust properties of the model.

Experimentally, the recent STM measurements on $\text{La}_2\text{PrNi}_2\text{O}_7$ thin films [22] have resolved two distinct superconducting gaps, with the larger gap being assigned

to the α band. In both Fermi surfaces, the gaps show minimum at $\theta = \pi/4$. Similar two-gap structure has been reported also in the bulk samples of $\text{La}_3\text{Ni}_2\text{O}_{7-\delta}$ under high-pressure [25]. Our theoretical findings above are fully consistent with these observations.

In summary, we have developed a microscopic theory addressing the superconducting gap structure in bilayer nickelates, based on the model in which itinerant $d_{x^2-y^2}$ electrons interact with localized $d_{3z^2-r^2}$ spins forming interlayer singlet dimers. Including orbital hybridization effects, we derived the effective band dispersions and Fermi surfaces consistent with ARPES data. We further derive the interactions between conduction electrons and local spins, including Kondo exchange processes.

The singlet-triplet excitations of the spin-dimer background mediate the interband Cooper pairing of the s_{\pm} -wave symmetry, with opposite signs of the order parameter on the α and β Fermi-surfaces. The pairing gaps acquire a sizable momentum anisotropy, originating from the nonlocal character of the Kondo exchange. Most of the results are presented as analytical expressions, which facilitate their comparison with experimental data.

Our theory captures two key experimental observations [22]. First, the α band hosts a larger superconducting gap than the β band, despite its smaller density of states. This hierarchy follows naturally from the interband nature of triplon-mediated pairing, where the gap amplitude on one Fermi surface sheet is controlled by the density of states on the other. Second, both gaps exhibit pronounced angular anisotropy with a minimum along the $k_x = k_y$ direction, as predicted by our theory. These findings strongly support the triplon-mediated pairing mechanism, helping to resolve the ongoing debate on superconductivity in bilayer nickelates.

We thank J. Chaloupka, M. Hepting, and B. Keimer for useful discussions. H. L. is supported by the National Natural Science Foundation of China under the Grant No. 12574066 and by the Fundamental Research Funds for the Central Universities under the Grant No. KG202501. G. Kh. acknowledges support from the European Research Council under Advanced Grant No. 101141844 (SpecTera).

[1] H. Sun, M. Huo, X. Hu, J. Li, Z. Liu, Y. Han, L. Tang, Z. Mao, P. Yang, B. Wang, J. Cheng, D.-X. Yao, G.-M. Zhang, and M. Wang, Signatures of superconductivity near 80 K in a nickelate under high pressure, *Nature* **621**, 493 (2023).
 [2] G. Wang, N. N. Wang, X. L. Shen, J. Hou, L. Ma, L. F. Shi, Z. A. Ren, Y. D. Gu, H. M. Ma, P. T. Yang, Z. Y. Liu, H. Z. Guo, J. P. Sun, G. M. Zhang, S. Calder, J.-Q. Yan, B. S. Wang, Y. Uwatoko, and J.-G. Cheng, Pressure-induced superconductivity in polycrystalline $\text{La}_3\text{Ni}_2\text{O}_{7-\delta}$, *Phys. Rev. X* **14**, 011040 (2024).

[3] E. K. Ko, Y. Yu, Y. Liu, L. Bhatt, J. Li, V. Thampy, C.-T. Kuo, B. Y. Wang, Y. Lee, K. Lee, J.-S. Lee, B. H. Goodge, D. A. Muller, and H. Y. Hwang, Signatures of ambient pressure superconductivity in thin film $\text{La}_3\text{Ni}_2\text{O}_7$, *Nature* **638**, 935 (2025).
 [4] G. Zhou, W. Lv, H. Wang, Z. Nie, Y. Chen, Y. Li, H. Huang, W.-Q. Chen, Y.-J. Sun, Q.-K. Xue, and Z. Chen, Ambient-pressure superconductivity onset above 40 K in $(\text{La,Pr})_3\text{Ni}_2\text{O}_7$ films, *Nature* **640**, 641 (2025).
 [5] Y. Liu, E. K. Ko, Y. Tarn, L. Bhatt, B. H. Goodge, D. A. Muller, S. Raghu, Y. Yu, and H. Y. Hwang, Superconductivity and normal-state transport in compressively strained $\text{La}_2\text{PrNi}_2\text{O}_7$ thin films, arXiv:2501.08022.
 [6] P. Puphal, T. Schäfer, B. Keimer, and M. Hepting, Superconductivity in infinite-layer and Ruddlesden-Popper nickelates, *Nat. Rev. Phys.* **8**, 70 (2025).
 [7] Z. Luo, X. Hu, M. Wang, W. Wú, and D.-X. Yao, Bilayer two-orbital model of $\text{La}_3\text{Ni}_2\text{O}_7$ under pressure, *Phys. Rev. Lett.* **131**, 126001 (2023).
 [8] Q.-G. Yang, D. Wang, and Q.-H. Wang, Possible s_{\pm} -wave superconductivity in $\text{La}_3\text{Ni}_2\text{O}_7$, *Phys. Rev. B* **108**, L140505 (2023).
 [9] Y.-F. Yang, G.-M. Zhang, and F.-C. Zhang, Interlayer valence bonds and two-component theory for high- T_c superconductivity of $\text{La}_3\text{Ni}_2\text{O}_7$ under pressure, *Phys. Rev. B* **108**, L201108 (2023).
 [10] Q. Qin and Y.-F. Yang, High- T_c superconductivity by mobilizing local spin singlets and possible route to higher T_c in pressurized $\text{La}_3\text{Ni}_2\text{O}_7$, *Phys. Rev. B* **108**, L140504 (2023).
 [11] Y.-B. Liu, J.-W. Mei, F. Ye, W.-Q. Chen, and F. Yang, s_{\pm} -wave pairing and the destructive role of apical-oxygen deficiencies in $\text{La}_3\text{Ni}_2\text{O}_7$ under pressure, *Phys. Rev. Lett.* **131**, 236002 (2023).
 [12] H. Oh and Y.-H. Zhang, Type-II $t - J$ model and shared superexchange coupling from Hund's rule in superconducting $\text{La}_3\text{Ni}_2\text{O}_7$, *Phys. Rev. B* **108**, 174511 (2023).
 [13] Z. Liao, L. Chen, G. Duan, Y. Wang, C. Liu, R. Yu, and Q. Si, Electron correlations and superconductivity in $\text{La}_3\text{Ni}_2\text{O}_7$ under pressure tuning, *Phys. Rev. B* **108**, 214522 (2023).
 [14] F. Lechermann, J. Gondolf, S. Bótzfel, and I. M. Eremin, Electronic correlations and superconducting instability in $\text{La}_3\text{Ni}_2\text{O}_7$ under high pressure, *Phys. Rev. B* **108**, L201121 (2023).
 [15] X.-Z. Qu, D.-W. Qu, X.-W. Yi, W. Li, G. Su, Hund's rule, interorbital hybridization, and high- T_c superconductivity in the bilayer nickelate, arXiv:2311.12769.
 [16] H. Sakakibara, N. Kitamine, M. Ochi, and K. Kuroki, Possible high- T_c superconductivity in $\text{La}_3\text{Ni}_2\text{O}_7$ under high pressure through manifestation of a nearly half-filled bilayer Hubbard model, *Phys. Rev. Lett.* **132**, 106002 (2024).
 [17] J. Chen, F. Yang, and W. Li, Orbital-selective superconductivity in the pressurized bilayer nickelate $\text{La}_3\text{Ni}_2\text{O}_7$: An infinite projected entangled-pair state study, *Phys. Rev. B* **110**, L041111 (2024).
 [18] C. Lu, Z. Pan, F. Yang, and C. Wu, Interplay of two E_g orbitals in superconducting $\text{La}_3\text{Ni}_2\text{O}_7$ under pressure, *Phys. Rev. B* **110**, 094509 (2024).
 [19] X.-W. Yi, W. Li, J.-Y. You, B. Gu, and G. Su, Unifying strain- and pressure-driven superconductivity in $\text{La}_3\text{Ni}_2\text{O}_7$: Suppressed charge and spin density waves and enhanced interlayer coupling, *Phys. Rev. B* **112**, L140504

- (2025).
- [20] G. Khaliullin and J. Chaloupka, Orbital order and superconductivity in bilayer nickelate compounds, *Phys. Rev. B* **113**, L041115 (2026).
- [21] J. Wang, Y.-F. Yang, Fermi liquid and isotropic superconductivity of Hund scenario for bilayer nickelates, arXiv:2507.19301.
- [22] S. Fan, M. Ou, M. Scholten, Q. Li, Z. Shang, Y. Wang, J. Xu, H. Yang, I. M. Eremin, and H.-H. Wen, Superconducting gap structure and bosonic mode in $\text{La}_2\text{PrNi}_2\text{O}_7$ thin films at ambient pressure, arXiv:2506.01788.
- [23] J. Shen, G. Zhou, Y. Miao, P. Li, Z. Ou, Y. Chen, Z. Wang, R. Luan, H. Sun, Z. Feng, X. Yong, Y. Li, L. Xu, W. Lv, Z. Nie, H. Wang, H. Huang, Y.-J. Sun, Q.-K. Xue, J. He, Z. Chen, Nodeless superconducting gap and electron-boson coupling in $(\text{La,Pr,Sm})_3\text{Ni}_2\text{O}_7$ films, arXiv:2502.17831.
- [24] W. Sun, Z. Jiang, B. Hao, S. Yan, H. Zhang, M. Wang, Y. Yang, H. Sun, Z. Liu, D. Ji, Z. Gu, J. Zhou, D. Shen, D. Feng, and Y. Nie, Observation of superconductivity-induced leading-edge gap in Sr-doped $\text{La}_3\text{Ni}_2\text{O}_7$ thin films, arXiv:2507.07409.
- [25] J. Guo, Y. Chen, Y. Wang, H. Sun, D. Hu, M. Wang, X. Huang, and T. Cui, Revealing superconducting gap in $\text{La}_3\text{Ni}_2\text{O}_{7-\delta}$ by Andreev reflection spectroscopy under high pressure, arXiv:2509.12601.
- [26] Z.-Y. Cao, D. Peng, S. Choi, F. Lan, L. Yu, E. Zhang, Z. Xing, Y. Liu, F. Zhang, T. Luo, L. Chen, V. T. A. Hong, S.-Y. Paek, H. Jang, J. Xie, H. Liu, H. Lou, Z. Zeng, Y. Ding, J. Zhao, C. Liu, T. Park, Q. Zeng, and H.-K. Mao, Direct observation of d-wave superconducting gap symmetry in pressurized $\text{La}_3\text{Ni}_2\text{O}_{7-\delta}$ single crystals, arXiv:2509.12606.
- [27] H. C. R. B. Bhatta, X. Zhang, Y. Zhong, and C. Jia, Structural and electronic evolution of bilayer nickelates under biaxial strain, arXiv:2502.01624.
- [28] B. Y. Wang, Y. Zhong, S. Abadi, Y. Liu, Y. Yu, X. Zhang, Y.-M. Wu, R. Wang, J. Li, Y. Tarn, E. K. Ko, V. Thampy, M. Hashimoto, D. Lu, Y. S. Lee, T. P. Devereaux, C. Jia, H. Y. Hwang, and Z.-X. Shen, Electronic structure of compressively strained thin film $\text{La}_3\text{PrNi}_2\text{O}_7$, arXiv:2504.16372.
- [29] S. Sachdev and R. N. Bhatt, Bond-operator representation of quantum spins: Mean-field theory of frustrated quantum Heisenberg antiferromagnets, *Phys. Rev. B* **41**, 9323 (1990).
- [30] T. Sommer, M. Vojta, and K. W. Becker, Magnetic properties and spin waves of bilayer magnets in a uniform field, *Eur. Phys. J. B* **23**, 329 (2001).
- [31] P. Coleman, *Introduction to Many-Body Physics* (Cambridge University Press, Cambridge, 2015), Chap. 16.